Applied Catalysis B: Environmental 188 (2016) 292–304

Contents lists available at ScienceDirect

Applied Catalysis B: Environmental

journal homepage: www.elsevier.com/locate/apcatb

Characterization and catalytic properties of $CuO/CeO_2/MgAl_2O_4$ for preferential oxidation of CO in H_2-rich streams

A. Elmhamdi [a], R. Castañeda [b], A. Kubacka [b], L. Pascual [b], K. Nahdi [a], A. Martínez-Arias [b,*]

[a] Laboratoire d'Application de la Chimie aux Ressources et Substances Naturelles et à l'Environnement, Faculté des Sciences de Bizerte, Université de Carthage, 7021 Zarzouna, Bizerte, Tunisie, Tunisia
[b] Instituto de Catálisis y Petroleoquímica, CSIC, Campus de Cantoblanco, C/Marie Curie 2, 28049 Madrid, Spain

ARTICLE INFO

Article history:
Received 23 December 2015
Accepted 3 February 2016
Available online 6 February 2016

Keywords:
Nanostructured $CuO/CeO_2/MgAl_2O_4$ catalysts
CO-PROX
DRIFTS
EPR
HREM
XEDS
XPS
TPR
Hydrogen

ABSTRACT

Catalysts of copper (1 wt.%) supported on a $CeO_2/MgAl_2O_4$ mixed support have been prepared by using different pH values (pH ~ 4, 8 and 10) in the impregnating solution of copper with the aim of favoring different situations of interaction between copper and the two support components. The catalysts have been characterized in detail by XRD, S_{BET} measurement, HREM and associated techniques, XPS, H_2-TPR and EPR which allows establishing a model of structural characteristics of the catalysts. The characterization results have been correlated with analysis of the catalytic properties of the samples for preferential oxidation of CO in a H_2-rich stream (CO-PROX) complemented by *operando*-DRIFTS. Important structural/chemical/catalytic differences as a function of the pH of the impregnating solution are revealed. These are explained on the basis of the characteristics of the interfaces formed between the different components present in each catalyst which basically determine the catalytic properties in each case.

1. Introduction

Production of H_2 for polymer fuel cells (PEMFC) is usually accomplished by a multi-step process that includes catalytic reforming of hydrocarbons or oxygenated hydrocarbons followed by water–gas shift (WGS) [1,2]. However, PEMFCs require hydrogen feed that is mostly free from CO, as otherwise the Pt based anode catalyst would be deactivated rapidly [2,3]. The high concentration of CO is brought down to less than 0.5 mol.%, through a two-stage water gas shift (WGS) reactor, in which CO is reacted with water to produce hydrogen and carbon dioxide [4]. Since the CO level is still much higher than a PEMFC anode can tolerate [4], it has to be selectively oxidized to bring its concentration to very low level (typically below 100 ppm) in excess of H_2 (and with the presence of H_2O and CO_2 in the feed), which is a current challenge in heterogeneous catalysis. Among different possibilities in this sense, the catalytic preferential oxidation of CO (CO-PROX) is considered as most simple and effective process to attain such goal [5–7].

The catalysts for CO-PROX reported in the scientific literature can be basically classified into three types: (i) noble metal catalysts based on Pt, Pd, Rh or Ir typically supported on Al_2O_3, SiO_2 or zeolites [6,7,8–17]; (ii) gold catalysts supported on different oxides like MnO_x, FeOx, TiO_2, Al_2O_3, NiO, MgO and SnO_2 [6,7,18–21]; (iii) several kinds of base metal oxide catalysts, such as the oxides of Cu, Mn, Co, Ni and Fe, either alone or in combination with other oxides [6,7,22–25]. Among the latter, catalysts combining copper and cerium oxides have demonstrated an important potential for the process, being able to compete with less economically interesting noble metal catalysts; in particular, they generally show higher selectivity at full CO conversion than catalysts based on platinum-group metals and they appear more resistant to the presence of CO_2 than catalysts based on gold [6,7,26]. The particular ability of copper-ceria catalysts for the CO-PROX process has been essentially attributed to the synergistic redox properties produced upon formation of copper oxide-ceria interfacial sites, which are considered to constitute the active sites for the CO oxidation reaction [27–31].

Further than the simple combination of copper and cerium oxides, it is interesting from a practical point of view to explore the properties of this type of catalysts when supported onto another functional material. Typically Al_2O_3, TiO_2, $MgAl_2O_4$ or SiO_2 are employed as supports for oxidation catalysts due to their high ther-

* Corresponding author.
E-mail address: amartinez@icp.csic.es (A. Martínez-Arias).

http://dx.doi.org/10.1016/j.apcatb.2016.02.011
0926-3373/

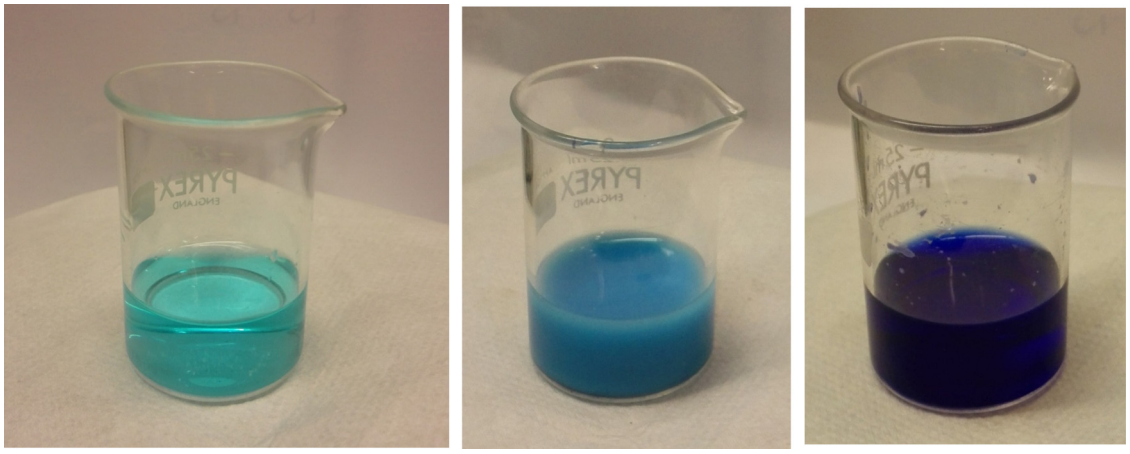

Fig. 1. Pictures of the copper impregnating solutions employed. Left: pH = 4.0, Center: pH = 8.0; Right: pH = 10.0.

mal stability, their relatively high specific surface area and/or their beneficial role in terms of resistance to poisons like sulfur or phosphorus [32–34]. Among them, $MgAl_2O_4$ is a support of high basicity with particular interest for mitigating deactivation by sulfur compounds which can be present as impurity in hydrocarbon reforming flows [33]. Another interesting point related to the use of ceria supported onto another material is related to the fact that the catalytic properties of supported ceria nanoparticles can be different than those of bulk ceria [35–37]. In particular, concerning the CO-PROX application of this type of catalysts, it has been observed that decreasing the particle size of ceria, which can be more or less easily achievable upon supporting it over another high surface area material, interesting new CO-PROX properties appear, as recently demonstrated [38]. Within this context, the present work explores a series of $CuO/CeO_2/MgAl_2O_4$ catalysts employed for CO-PROX. Different pH values (pH ~ 4.0, 8.0 and 10.0) were selected for the impregnating aqueous solution employed for depositing the copper on preformed $CeO_2/MgAl_2O_4$ support and considering point of zero charge (PZC) values for the two support components of 6.8 and 9.0 for CeO_2 and $MgAl_2O_4$, respectively [39,40]. Thus, selected different pH values could in principle favor the deposition of copper onto one or another support component [41]; in turn, the pH can also affect the type of contacts established between active copper and cerium oxide components [42,43]. The study involves a multitechnique characterization along with catalytic activity tests complemented by *operando*-DRIFTS spectroscopy under CO-PROX conditions with the aim of establishing structure/activity relationships for this type of catalyst/process.

2. Experimental

2.1. Sample preparation

$MgAl_2O_4$ was prepared by a sol-gel method by adding citric acid in excess ($3 \times [Al^{3+} + Mg^{2+}]$) to an aqueous solution of magnesium and aluminum chlorides with the appropriate molar ratios. The mixture was kept under stirring at 80 °C until complete evaporation of the liquid. The resulting gel was dried overnight at 100 °C and finally calcined at 900 °C for 4 h. CeO_2 (10.0 wt.%) was deposited onto the $MgAl_2O_4$ support by the microemulsion method. Two reverse microemulsions were mixed for this purpose. The first was prepared by including cerium (III) nitrate hexahydrate into its aqueous phase and dispersing the $MgAl_2O_4$ in it; the second one included tetramethylammonium hydroxyde pentahydrate (TMAH) as precipitating base into its aqueous phase. The microemulsions were in any case prepared by using *n*-heptane as major organic phase, Triton X-100 (Aldrich) as surfactant and hexanol as co-surfactant in volumes similar to those employed in previous works and in which further details of the preparation can be found [29,44]. After centrifugation and decantation the resulting solid was rinsed with methanol, then dried at 120 °C for 24 h and finally calcined in air at 500 °C for 2 h. Three catalysts of copper supported on $CeO_2/MgAl_2O_4$ were prepared by incipient wetness impregnation of the $CeO_2/MgAl_2O_4$ support using aqueous solutions of $Cu(NO_3)_2{\cdot}3H_2O$ (to give a final copper loading of 1 wt.% in any case) at pH ~ 4.0, 8.0 and 10.0. The former corresponds to natural pH of the copper nitrate impregnating solution employed. Aqueous concentrated ammonium hydroxide was added in the amount required in order to achieve basic pH values in this impregnating solution. A pH-meter (Crison MicropH 2001) was employed in order to adjust corresponding pH values in each case. Pictures of the impregnating solutions employed are shown in Fig. 1. As shown, the solution evolves from clear light blue at pH = 4.0 to a milky opaque light blue dispersion at pH = 8.0 and finally a deep blue solution at pH = 10.0. The three resulting materials were dried overnight at 120 °C and subsequently calcined in air at 500 °C for 2 h. These samples will be referred to as Cu/Ce/MgAl-x with x = 4, 8 and 10, corresponding to the pH value of the impregnating solution employed in each case.

Reference samples of copper supported on separate support components CeO_2 (prepared using the same microemulsion procedure as exposed above, except for the absence of $MgAl_2O_4$ in the microemulsion of the cerium salt) and $MgAl_2O_4$ were prepared by incipient wetness impregnation of the CeO_2 and of the $MgAl_2O_4$ support using an aqueous solution of $Cu(NO_3)_2{\cdot}3H_2O$ (to give a final copper loading of 1 wt.%) at pH = 8 (this was selected on the basis of catalytic activity results previously obtained for the series of $CeO_2/MgAl_2O_4$-supported samples, *vide infra*) prepared upon addition of the adequate amount of aqueous ammonia, as exposed above. The two resulting materials were dried overnight at 120 °C and subsequently calcined in air at 500 °C for 2 h. These samples will be denoted hereafter as Cu/Ce-8 and Cu/MgAl-8, respectively.

2.2. Techniques

The chemical composition of the catalysts was examined by inductively coupled plasma atomic emission spectroscopy (ICP-AES) chemical analysis (Optima 3300 DV Perkin Elmer equipment). Quantitative precipitation of the cerium and copper amounts as expected for the nominal amounts employed were evidenced in any case.

The specific surface area of the calcined catalysts was determined by the BET method upon fitting of N_2 adsorption isotherms performed with a Micromeritics 2100 automatic apparatus at liquid nitrogen temperature. The catalysts were degassed at 140 °C in vacuum for 12 h before measurement of the corresponding isotherms.

Powder XRD patterns of the samples were recorded on a XíPert Pro PANalytical diffractometer using CuKα radiation (λ = 1.5418 Å, 45 kV, 40 mA), using a 0.02° step size and 2s counting time per point. Analysis of the diffraction peaks was done with the computer program ANALYZE Rayflex Version 2.293.

The X-ray photoelectron spectra (XPS) of the catalysts were collected using a Specs Gmbh spectrometer under UHV conditions ($P \approx 10^{-10}$ mbar) and using Mg Kα radiation and a Phoibos 150 9MCD energy analyzer. During data processing of the XPS spectra, the binding energy values were estimated by using as reference the C 1s peak of contaminant carbon at 285.0 eV; correct correction was further checked by adjusting the characteristic u'" peak of Ce 3d to 917.0 eV [45]. The CasaXPS MFC application software package was used for data analysis.

High resolution transmission electron microscopy (HRTEM) data as well as scanning transmission electron microscopy-high angle annular dark field (STEM-HAADF) images and X-ray energy dispersive spectra (XEDS) were recorded on a JEOL TEM/STEM 2100F field emission gun transmission electron microscope operating at 200 kV and equipped with an EDS spectrometer Oxford INCA X-sight system. XEDS analysis was performed in STEM mode. Specimens were prepared by depositing small portions of the samples to be investigated from ethanol dispersion onto a nickel grid supporting a perforated carbon film.

The electron paramagnetic resonance (EPR) measurements were done with a Bruker ER200D spectrometer operating in the X-band and calibrated with a DPPH standard. The spectra were recorded at −196 °C using a conventional spectroscopic quartz tube cell employed for studies of solid samples. Aliquots of the sample (between 20 and 30 mg) were thoroughly treated under high vacuum conditions at room temperature prior to measurement. Copper sulfate was used as standard for quantitative estimation.

Temperature programmed reduction (TPR) was measured in a flow system using 5% H_2/He premixed gas with flow rate of 30 mL min^{-1}. 100 mg of catalyst was placed into a glass tube and pretreated under 10% O_2/He at 500 °C for 1 h using 100 mL min^{-1} flow rate and 10 °C min^{-1} ramp. The sample was then cooled to room temperature, thoroughly purged with Ar and after switching to the reducing gas mixture it was heated up to 500 °C using 10 °C min^{-1} ramp. A quadrupole mass spectrometer Pfeiffer Omnistar was used as detection system.

The catalysts calcined in situ (under oxygen diluted in Ar at 500 °C) were tested in a glass tubular catalytic reactor for their activity under an atmospheric pressure flow (using mass flow controllers to prepare the reactant mixture) of 1% CO, 1.25% O_2 and 50% H_2 (Ar balance), at a rate of 1000 cm^3 min^{-1} g^{-1} (roughly corresponding to 80,000 h^{-1} GHSV) and using a heating ramp of 5 °C min^{-1}. Analysis of the feed and outlet gas streams was done by gas infrared (Bruker Equinox 55 FTIR spectrometer, coupled to a multiple reflection transmission cell—Infrared Analysis Inc. "long path gas minicell", 2.4 m path length, ca. 130 cm^3 internal volume) and mass spectrometry (Pfeiffer Omnistar). No products other than those resulting from CO or H_2 combustion (i.e. CO_2 and H_2O; note that possible contributions of WGS or reverse WGS must be residual under the conditions employed and, if at all, would take place only at temperatures higher than ca. 200 °C over this type of catalysts [46]) were detected in the course of the runs, in agreement with previous results on catalysts of this type [29]. On this basis, values of percentage conversion and selectivity in the CO-PROX process

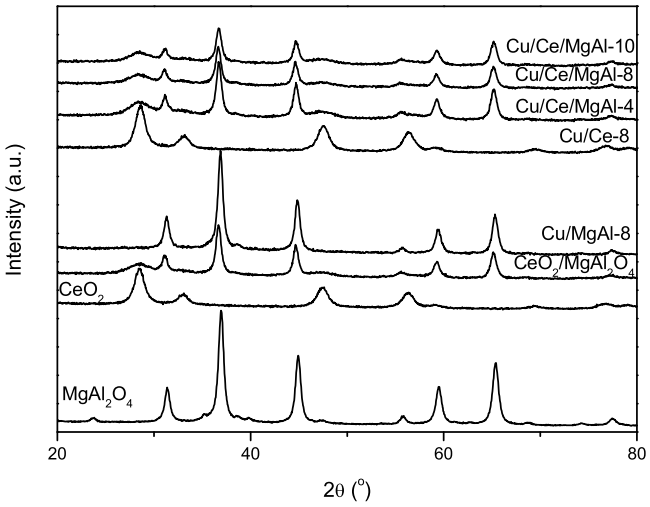

Fig. 2. X-ray diffractograms for the indicated samples.

are defined as:

$$X_{CO} = \frac{F_{CO}^{in} - F_{CO}^{out}}{F_{CO}^{in}} \times 100; S_{CO2}$$

$$= \frac{X_{co}}{2.5X_{O2}} \times 100; X_{O2} = \frac{F_{O2}^{in} - F_{O2}^{out}}{F_{O2}^{out}} \times 100$$

where X and S are percentage conversion and selectivity, respectively, and F is the (inlet or outlet) molar flow of the indicated gas.

Operando-DRIFTS experiments were carried out using a Bruker Equinox 55 FTIR spectrometer fitted with an MCT detector. The DRIFTS cell (Harrick) was fitted with CaF_2 windows and a heating cartridge that allowed samples to be heated to 500 °C. Aliquots of ca. 100 mg were calcined in situ (in a similar way as employed for the catalytic tests) and then cooled to room temperature under diluted oxygen before introducing the reaction mixture and heating under a 5 °C min^{-1} ramp, recording typically one spectrum (accumulating 20 scans) every 20 °C. The gas mixture (1% CO + 1.25% O2 + 50% H_2 in He, similar to that employed for the catalytic activity tests) was prepared using mass flow controllers with ca. 100 cm^3 min^{-1} passing through the catalyst bed at atmospheric pressure, which corresponds to conditions similar to those employed for the activity tests performed with the tubular reactor.

3. Results and discussion

3.1. Characterization

BET specific surface areas of 65, 66 and 65 m^2 g^{-1} were obtained for Cu/Ce/MgAl-4, Cu/Ce/MgAl-8 and Cu/Ce/MgAl-10, respectively, slightly higher than that obtained for the parent $MgAl_2O_4$ support (61 m^2 g^{-1}). Cu/Ce-8 and Cu/MgAl-8 reference catalysts displayed S_{BET} = 110 and 57 m^2 g^{-1}, respectively.

The X-ray diffractograms obtained for the various catalysts and supports employed are shown in Fig. 2. The $MgAl_2O_4$ and CeO_2 supports show peaks corresponding to those expected for the spinel and fluorite phases of these compounds, respectively. In the case of the mixed support $CeO_2/MgAl_2O_4$, the most intense (1 1 1) diffraction of CeO_2 fluorite phase at ca. 28.4° (in 2θ) is apparent. This is appreciably wider relatively to that observed for the CeO_2 support, which reveals a lower crystal size for this phase, (using the Scherrer equation) ca. 7.5 and 3.5 nm in CeO_2 and $CeO_2/MgAl_2O_4$, respectively. As for the copper catalysts, no appreciable differences are found with respect to the diffractograms observed for the cor-

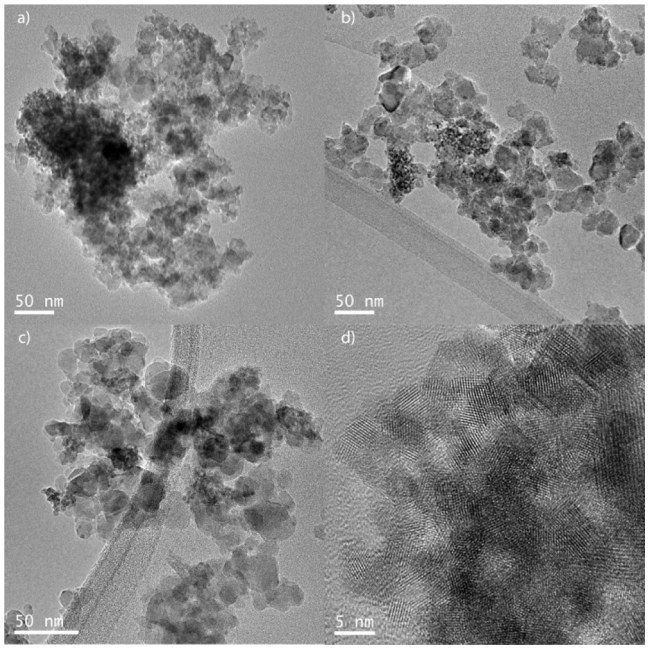

Fig. 3. TEM micrographs of Cu/Ce/MgAl-4 (a), Cu/Ce/MgAl-8 (b) and Cu/Ce/MgAl-10 (c); HRTEM image of the CeO_2 particles in Cu/Ce/MgAl-4.

responding supports. This indicates that the copper would appear in a highly dispersed state in either case (note that in any case, the most intense peaks corresponding to CuO are expected to appear at $2\theta \approx 36^\circ$ and 39°, the latter would appear at a position apparently free from overlapping with peaks originating from the support; in any case, it must be considered that the copper content, and its diffraction cross section with respect to ceria, is relatively low as to produce relatively intense peaks).

To complement the structural analysis of the $CuO/CeO_2/MgAl_2O_4$ catalysts, we examined the three samples by HRTEM, STEM-HAADF and XEDS. Multiple HRTEM as well as STEM-HAADF micrographs along with XEDS spectra have been recorded and thus sufficiently representative data was collected. Let us first discuss the CeO_2 phase. Fig. 3 shows direct bright field TEM images of the three catalysts. The presence of nanoparticles in which lattice fringes appear at higher magnification and whose interplanar distances are compatible with the presence of the fluorite ceria phase are detected in these images (Fig. 3d). The average crystal size estimated for them appears close to the one determined from XRD of CeO_2 particles (ca. 3 nm). These CeO_2 nanoparticles apparently form aggregates in some case but they appear also as dispersed entities all over the $MgAl_2O_4$ support.

In order to determine the particle size distribution of the CeO_2 particles for each catalyst, we have acquired STEM-HAADF micrographs (Fig. 4) which facilitates the identification of the CeO_2 phase due to the brighter contrast of Ce atoms present in the sample. Assuming the CeO_2 particles as spheres and measuring only the ones which are sufficiently isolated we can represent the radii vs the frequency (insets in Fig. 4). The results are well fitted to a Gaussian curve and display a relatively narrow distribution. From the fit we obtain the mean value and the standard deviation for each sample: 3.4 ± 1.9 nm for Cu/Ce/MgAl-4, 2.5 ± 1.3 nm for Cu/Ce/MgAl-8 and 2.7 ± 1.3 nm for Cu/Ce/MgAl-10. We thus find some decrease of the CeO_2 particle size upon increasing the pH of the impregnating solution.

Regarding the CuO, the presence of this phase was detected when we carried out XEDS analysis in TEM mode but the localization of CuO particles by means of TEM/STEM imaging was not possible. This was mainly because of the small concentration of this phase in the catalyst (1 wt.%). Also the low atomic number of Cu (Z = 29) compared to Ce (Z = 58) added to the difficulty in the detection. XEDS analysis and elemental mapping are thus crucial in order to identify the localization of this phase for each sample. To visualize the different Cu distribution, we have thus obtained STEM-HAADF images together with the elemental maps of Al, Ce and Cu present in each sample. On the whole, our results (Fig. 5) indicate that for Cu/Ce/MgAl-4 and Cu/Ce/MgAl-10, Cu is predominantly found within the CeO_2 aggregates. In contrast, in the case of Cu/Ce/MgAl-8 the concentration of Cu is not linked to the Ce particles and appears rather homogeneous over the whole support. In the case of Cu/Ce/MgAl-8, we show an area where Cu is clustering (form aggregates), which does not seem to be the usual case. Moreover, by means of XEDS analysis, several regions (of approximately 50 nm) with and without CeO_2 aggregates (clusters) were analyzed in the three samples, which confirm this result. To conclude, the results indicate that in the case of Cu/Ce/MgAl-8 the CuO phase shows no preference for depositing onto any of the phases present and a more homogeneous distribution of the CuO phase between both CeO_2 and $MgAl_2O_4$ components is achieved.

EPR spectra obtained at $-196\,^\circ C$ for the three $CuO/CeO_2/MgAl_2O_4$ samples are displayed in Fig. 6. Different signals attributable to paramagnetic Cu^{2+} entities are detected. Most prominent features present a shape characteristic of species with an axial (or near axial) symmetry with $g_{||} > g_\perp > g_e$ and four-line hyperfine splitting due to the interaction of the unpaired electrons with nuclei of spin $I = 3/2$ (signals type C). Two signals of this

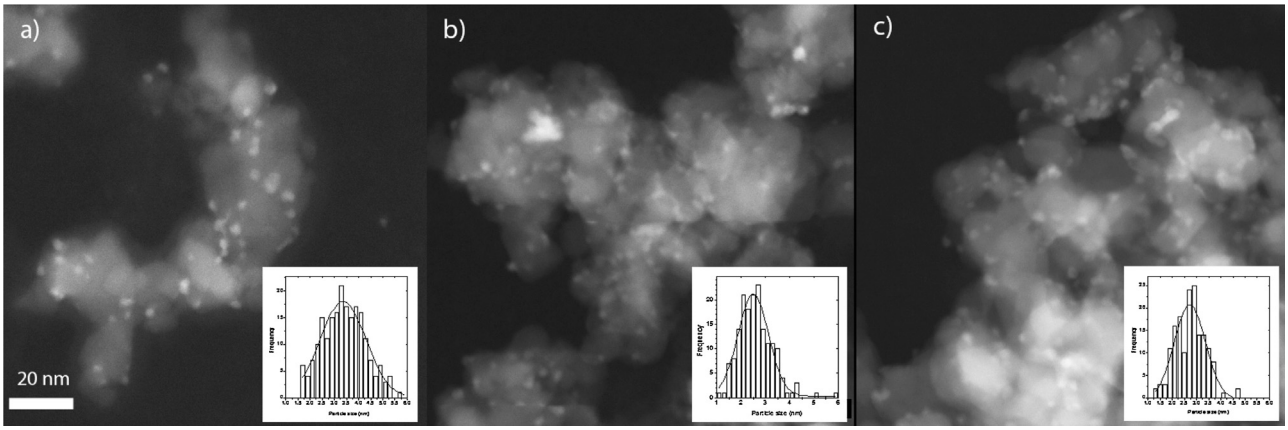

Fig. 4. STEM-HAADF micrographs of Cu/Ce/MgAl-4 (a), Cu/Ce/MgAl-8 (b) and Cu/Ce/MgAl-10 (c); respective particle size distribution of the CeO_2 particles (see main text) are shown in the insets.

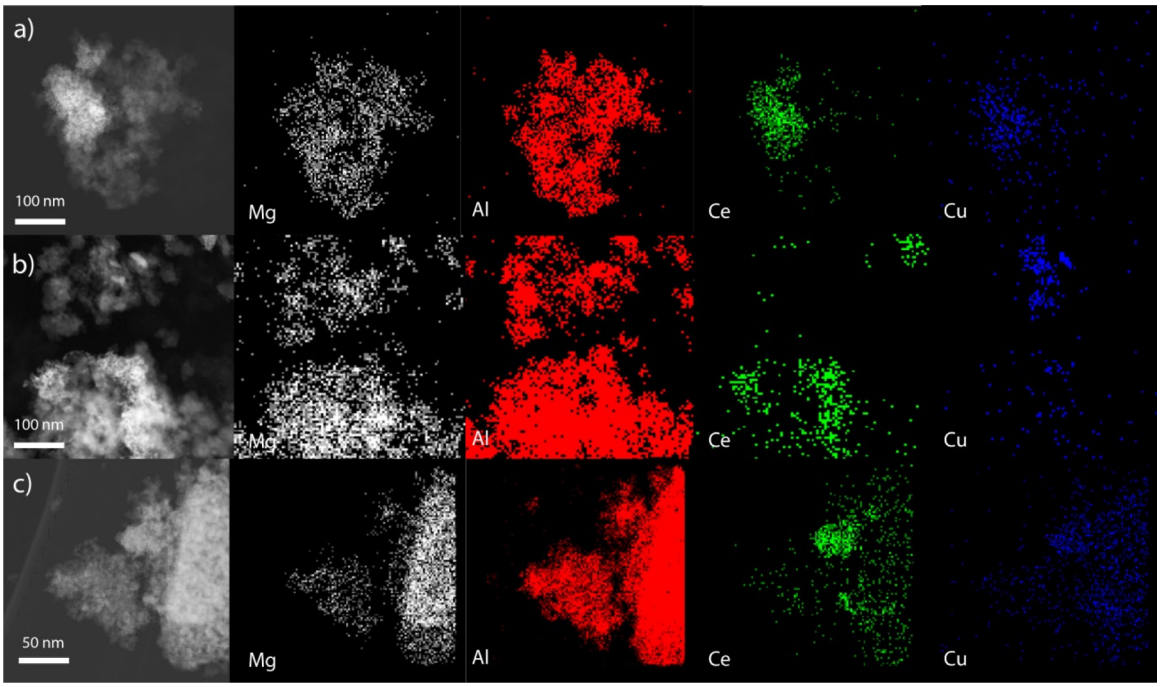

Fig. 5. STEM-HAADF micrographs and elemental XEDS mappings of Mg, Al, Ce and Cu for Cu/Ce/MgAl-4 (a), Cu/Ce/MgAl-8 (b) and Cu/Ce/MgAl-10 (c).

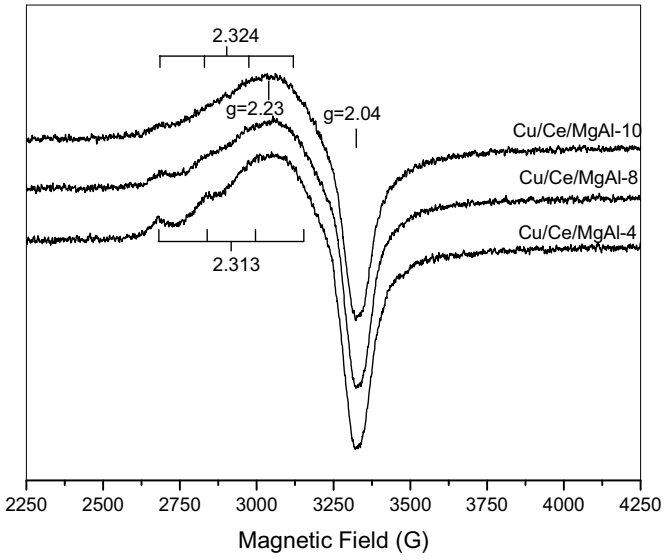

Fig. 6. EPR spectra at −196 °C of the indicated samples.

type are observed which differ in their $g_{||}$ and $A_{||}$ (Cu) values (C_1: $g_{||} = 2.313$, $A_{||}$ (Cu) = 154.0 G − 16.6 × 10^{-3} cm^{-1} −; C_2: $g_{||} = 2.324$, $A_{||}$ (Cu) = 145.0 G − 15.70 × 10^{-3} cm^{-1} −). In any case, they show $g_{\perp}$ close to 2.04 although hyperfine splitting cannot be resolved for this component. Signals C_1 and C_2 correspond to isolated Cu^{2+} species characterized by axial spectra with resolved Cu hyperfine features [47–49]. The spin Hamiltonian parameters obtained suggest that the geometry around Cu^{2+} can be generally described as square pyramidal [47]. They display $g_{||}$ values which appear greater than observed for this type of species when supported on pure ceria although they are closer to those detected over alumina [47–49]. This suggests these isolated Cu^{2+} species could form over the $MgAl_2O_4$ component in each case. The different $g_{||}$ value observed for them indicates in any case a somewhat different chemical environment around each Cu^{2+} cation. Signal C_1 appears characteristic for the sample prepared at pH = 4 and signal C_2 for the one prepared at pH = 10 with the sample prepared at pH = 8 apparently presenting both signals. Such isolated Cu^{2+} species constitute in any case a minor contribution to the whole spectrum in each case. Most of the intensity corresponds for the three samples to a major signal B onto which signals type C appear overlapped and which is characterized by a broad asymmetric shape showing maximum and minimum at g ∼ 2.23 and 2.04, respectively. This is attributed to dipolar, interacting Cu^{2+} ions [47,48], probably forming nano-sized copper particles not sufficiently big or crystalline as to form CuO crystals for which antiferromagnetic interactions would prevent EPR observation of the Cu^{2+} cations [47,48,50]. In this sense, quantitative estimation of the intensity of the spectra obtained shows that only ca. 52% of the whole copper is detected by EPR for Cu/Ce/MgAl-4 (and ca. 51 and 50% for Cu/Ce/MgAl-8 and Cu/Ce/MgAl-10, respectively), indicating that a significant part of the copper remains as EPR-silent in any of the samples. This can be due to either the presence of antiferromagnetically coupled Cu^{2+} cations (as in well crystallized CuO [50]) or diamagnetic states of copper (like Cu^{+}). This point will be further substantiated below when examining XPS results.

H_2-TPR experiments were performed in order to explore the redox properties of the three $CuO/CeO_2/MgAl_2O_4$ samples, Fig. 7. Basically two reduction peaks are apparent below 400 °C. The first one, at lower temperature, appears at ca. 250 °C for Cu/Ce/MgAl-4 and Cu/Ce/MgAl-8 and 270 °C for Cu/Ce/MgAl-10. A second wider peak is apparent at higher reduction temperature for the three samples. It appears centered at ca. 310 °C and somewhat more intense for Cu/Ce/MgAl-8 while it appears at slightly higher temperature and less poorly defined for Cu/Ce/MgAl-4 and it appears shifted to ca. 340 °C for Cu/Ce/MgAl-10. These reduction peaks appearing at relatively low temperature are characteristic for the reduction of dispersed copper oxide entities [34,51], with (if contacting ceria entities) concomitant reduction of interfacial cerium cations typically taking place too [52]. The peak at lower temperature can be due to the reduction of highly dispersed copper oxide entities promoted by their contact with ceria while the peak at higher temperature can be due to less dispersed copper oxide entities of bigger

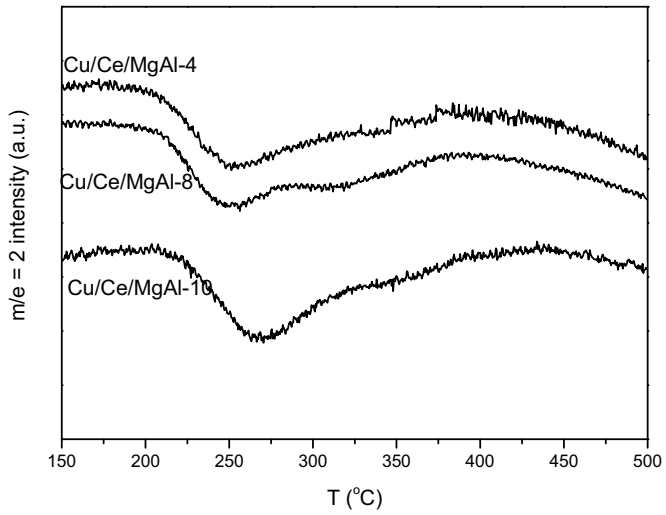

Fig. 7. H_2 evolution observed during H_2-TPR runs over the indicated catalysts.

Table 1
Summary of XPS data for the indicated catalysts in their initial calcined state.

catalyst	Cu $2p_{3/2}$ BE (eV)	[Ce]/([Ce]+[Al])[b]	[Cu]/([Cu]+[Ce]+[Al])[b]
Cu/Ce/MgAl-8	933.6 (60.2)[a] 935.2 (39.8)	0.0449	0.0192
Cu/Ce/MgAl-10	933.6 (77.5) 935.4 (22.5)	0.0430	0.0146

[a] Values between parentheses correspond to relative percentage of corresponding signal.
[b] Atomic ratios. Sensitivity factors employed for the estimation were taken from the work of Wagner et al. [56]. Cu $2p_{3/2}$, Ce 3d and Al 2p (signal at ca. 74 eV) spectra employed for this estimation.

size or non-promoted by interaction with ceria entities. On the other hand, the H_2 consumption observed above 400 °C is most likely related to the reduction of ceria entities. This appears also somewhat shifted to higher temperature for Cu/Ce/MgAl-10 which suggests a lower promoting effect by reduced copper entities on ceria reduction for this catalyst.

The surface of the $CuO/CeO_2/MgAl_2O_4$ catalysts prepared at pH = 8 and 10 (selected on the basis of their differing catalytic properties, as will be explored below) was examined by XPS. The spectra of Ce 3d, Cu $2p_{3/2}$ and O 1s binding energy regions of the two samples are shown in Fig. 8. Spectra in the Ce 3d region are similar to those observed for CeO_2 nanosized samples [53,54]. They basically exhibit a set of two doublets which correspond to a deconvolution into eight peaks labelled as u (u–u''') for $3d_{3/2}$ and v (v-v''') for $3d_{5/2}$. Among them, the doublet v'/u' is considered as the fingerprint of the presence of Ce^{3+} (note this is a simplification since they correspond only to the centre in each case of most intense peak or set of peaks observed for Ce_2O_3 [44,55]) whereas the other peaks are attributed to Ce^{4+} [44,55]. The main difference between the two samples in this zone is related to the higher relative contribution of Ce^{3+} features to the spectrum for Cu/Ce/MgAl-10 which reveals a higher reduction degree of cerium in this sample (20.8% of Ce^{3+} with respect to the whole cerium present in the sample, as compared to 11.5% of Ce^{3+} estimated for Cu/Ce/MgAl-8).

Concerning the Cu $2p_{3/2}$ zone, it shows for both samples two main peaks at ca. 933.6 and 935.4–935.2 eV along with less intense satellite peaks around 944–942 eV, [56] Fig. 8 and Table 1. According to Wagner and Moretti, the binding energy (BE) position is strongly sensitive not only to the valence state of copper but also to the chemical environment of the copper species since not only initial state but also final state effects can strongly affect it [57,58]. In this sense, a literature survey shows that copper species in well dis-

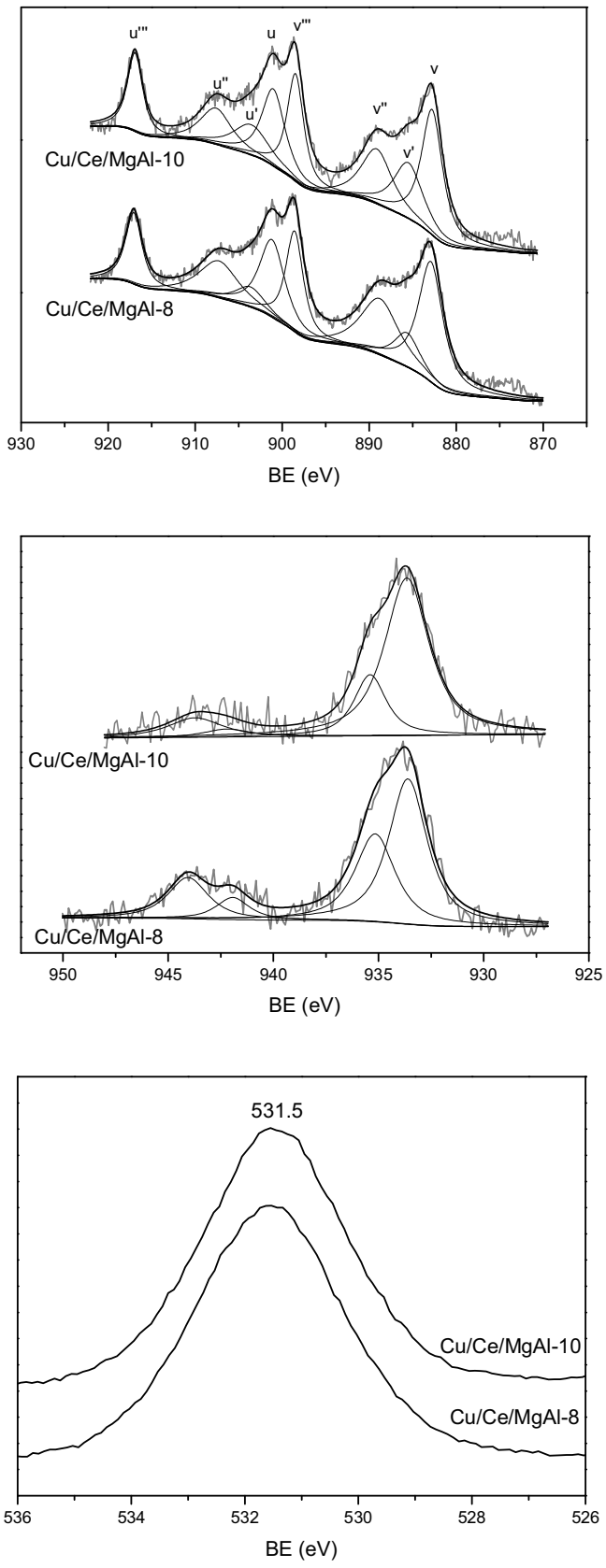

Fig. 8. XPS spectra for the indicated catalysts in Ce 3d (top), Cu $2p_{3/2}$ (middle) and O1s (bottom) regions.

persed calcined catalysts of copper supported on γ-Al_2O_3 typically display Cu $2p_{3/2}$ BE at 935.0–934.5 eV [59–61]. This contrasts with the position observed for analogous catalysts dispersed on CeO_2 in which the interaction with the support shifts the BE to lower energy and the dispersed copper species in the calcined catalysts typically yield values between 934.5 and 933.0 eV [29,48,59,60]. It is therefore tempting to attribute the peaks at ca. 933.6 and 935.4–935.2 eV to copper species in contact with the CeO_2 and $MgAl_2O_4$ components of the support, respectively. Note in this sense that their respective contributions to the spectra (higher relative contribution of the peak at 933.6 eV in Cu/Ce/MgAl-10 with respect to Cu/Ce/MgAl-8, Table 1) would qualitatively agree with the results of elemental XEDS mappings described above (Fig. 5). We cannot however discard that the different environment of the copper species is simply related to a hydroxide-like one for the peak at ca. 935.4–935.2 eV and an oxidic-like one for that at 933.6 eV irrespective of the support component with which they are in contact [62]. Unfortunately, the analysis of the O 1s zone does not allow discerning between these two possibilities. As shown in Fig. 8, a relatively wide peak centred at ca. 531.5 eV is observed in this zone for the two catalysts. This is similar to the BE position of bulk oxygen in $MgAl_2O_4$ [63], which would provide the main contribution to the spectra in agreement with the stronger surface contribution of this support component to the spectra (see atomic ratios collected by Table 1). Oxygen species from hydroxide species would yield a BE close to such value and cannot eventually be distinguished from them [53]. In turn, bulk oxygen from the other major component of the catalysts (CeO_2) would appear at 530.0–529.5 eV [53,59]. On the whole, the diversity of oxygen species (some carbonate-type species also present, as examined below) which can be present in the multicomponent catalyst explains the important width observed for these O 1s spectra which would result from convolution of the various possible contributions. Concerning the valence state of copper, both peaks appear at positions attributable to Cu^{2+} species [48,58–61]. It must in any case be taken into account that determination of the valence state of copper on the basis of only Cu 2p BE position is not straightforward. Thus, for instance, depending on their chemical environment which basically determines how final state effects affect to their BE [57,58], Cu^{2+} species could appear in the 935.5–933.5 BE range while Cu^{+} species could appear in the 933.8–932.5 BE range [48,54]. Typically, the use of corresponding Cu LMM Auger spectra provides a help in this sense and joint consideration of them along with corresponding Cu 2p XPS spectra is most useful in this sense. However, unfortunately, analysis of the Cu LMM Auger zone of the spectra does not allow obtaining further details in this case since the spectra (not shown) appear very broad and poorly defined in this zone. Alternatively, hints on the valence state of copper can be achieved from analysis of the relative contribution of satellite peaks at 944–942 eV since such peaks are exclusively related to the Cu^{2+} state of copper. In this respect, a different ratio between satellite and main Cu $2p_{3/2}$ peaks is observed (0.26 and 0.16 for Cu/Ce/MgAl-8 and Cu/Ce/MgAl-10, respectively), which indicates the presence of a higher relative amount of Cu^{2+} species in the former; i.e. apparently a part of the copper becomes stabilized in a reduced state for Cu/Ce/MgAl-10. Another difference between the two samples is noted in the atomic ratios collected by Table 1. These indicate a relatively higher dispersion degree of copper in Cu/Ce/MgAl-8 according to the higher [Cu]/([Cu]+[Ce]+[Al]) observed for it; note that the similarity observed in the [Ce]/([Ce]+[Al]) atomic ratio obtained for the two samples is in agreement with having similar dispersion degree of ceria in them, as expected from similar size for this component in these two samples according to STEM-HAADF investigation (Fig. 4).

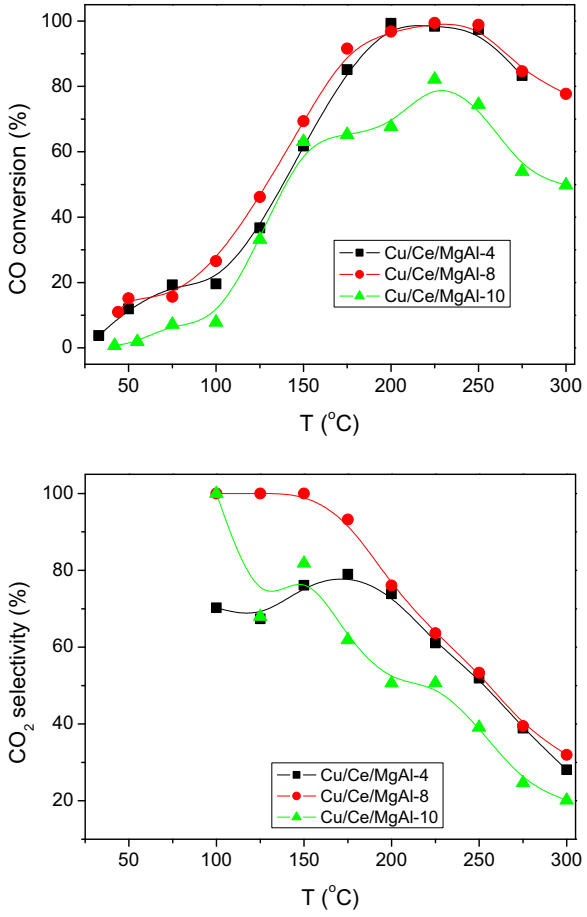

Fig. 9. Activity data obtained under CO-PROX conditions (1% CO, 1.25% O_2 and 50% H_2 in He) for the indicated catalysts.

3.2. Catalytic properties

Activity data for the three $CuO/CeO_2/MgAl_2O_4$ catalysts under CO-PROX conditions are shown in Fig. 9. Significant differences are observed between them. Cu/Ce/MgAl-8 is the one showing best general performance in terms of both CO conversion and selectivity to CO_2. In turn, Cu/Ce/MgAl-4 displays somewhat poorer CO oxidation activity and selectivity to CO_2 although, as Cu/Ce/MgAl-8, it is still able to keep a window of CO conversion close to 100% between 200 and 250 °C. In contrast, Cu/Ce/MgAl-10 displays a poor activity for the process both in terms of CO conversion and CO_2 selectivity.

Taking into account that optimum performance is achieved for the $CuO/CeO_2/MgAl_2O_4$ catalyst prepared at pH = 8, two reference catalysts were prepared by using $MgAl_2O_4$ and CeO_2 as supports and using the copper solution or dispersion prepared at such pH (Fig. 1) to impregnate the two supports, as described in the Experimental part. The main objective is to explore the catalytic properties of copper entities interacting separately with every one of the support components in order to achieve further information about the catalytic behavior of the more complex $CuO/CeO_2/MgAl_2O_4$ catalysts. Fig. 10 shows the activity data obtained over these two reference systems. Cu/Ce-8 displays the highest CO oxidation activity amongst the catalysts tested. It reaches CO conversion close to 100% at 125 °C and is able to keep a relatively high CO conversion level up to 250 °C. In contrast, Cu/MgAl-8 displays the worst behavior for the process among the catalysts examined in this study exhibiting only ca. 70% as maximum CO conversion at 275 °C and showing also relatively poor CO_2 selectivity during the whole run.

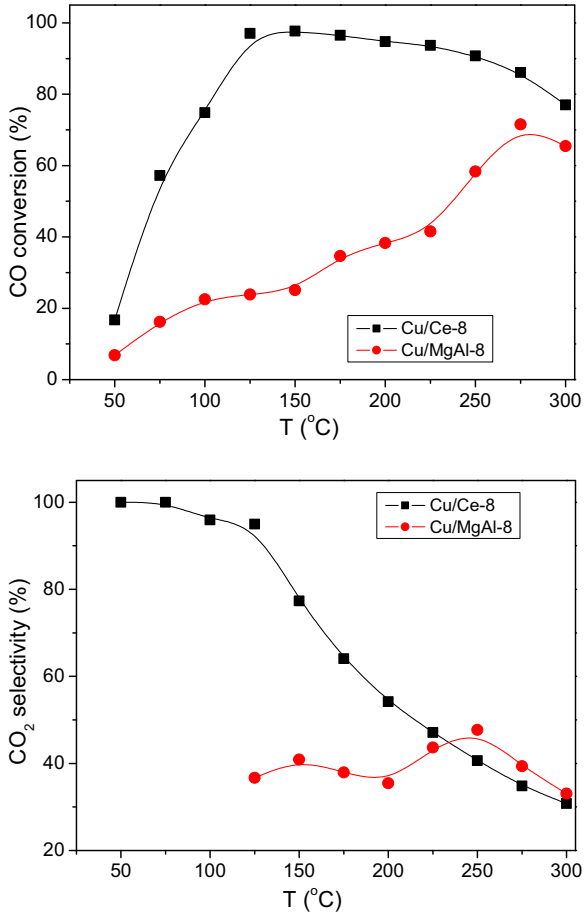

Fig. 10. Activity data obtained under CO-PROX conditions (1% CO, 1.25% O_2 and 50% H2 in He) for the indicated catalysts.

In order to analyze in detail the processes taking place over the catalysts during the course of the CO-PROX reaction, the results of catalytic activity have been complemented by *operando*-DRIFTS-MS. In first place, we examine the results obtained over the reference samples with the intention of isolating the behavior of the copper species under interaction with a single support component. Figs. 11 and 12 display the spectra obtained over Cu/Ce-8 and Cu/MgAl-8 samples, separated in the three regions in which changes are produced as a consequence of the interaction with the reactant mixture. Fig. 13 displays the evolution of CO_2 and H_2O during the course of the process and which reflect CO and H_2 oxidation activity, respectively, taking place over the two reference catalysts.

Attribution of the bands observed in the spectra is based on previous work to which the reader is referred to for details [64–67]. In the case of Cu/Ce-8 different bands corresponding to hydroxyl species appear in the 3800–2800 cm^{-1} spectral zone: isolated ones giving sharp bands in the 3720–3600 cm^{-1} range and associated species giving a broad band extending from ca. 3800 to 2800 cm-1 and with a maximum at ca. 3260 cm^{-1}. The spectral zone below 1700 cm^{-1} exhibits bands due to carbonate or related species. Most intense peaks in this zone are ascribed to bidentate carbonates at ca. 1575 and 1300 cm^{-1}. Mono- or tri-dentate carbonate species (controversy exists with respect to coordination state of this type of carbonate [65–67]) showing the stretching bands of the terminal CO bonds at ca. 1475 and 1350 cm-1 are also detected. In turn, a band at 1216 cm^{-1}, along with that at 1393 cm^{-1} and a shoulder at ca. 1600 cm^{-1} as well as a band at ca. 3620 cm^{-1} (related to O—H stretching in the complex) are attributed to hydrogen carbonate species. Bands at ca. 1510 and 1371 cm-1 along with those appearing at 2949 and 2846 cm-1 indicate the formation of formate species for T > 260 °C; this is typically correlated with onset of a residual WGS process [29]. The third spectral zone (at intermediate frequencies) shows the formation of carbonyl species giving rise to an intense band at ca. 2114–2104 cm^{-1}. Typically carbonyl bands around 2110 cm^{-1} appear upon interaction of this type of catalyst with CO and are attributed to Cu^+ carbonyls on the basis of their relatively large thermal stability [64]. The relatively low frequency of the carbonyl produced just after contact with the reactant mixture at 23 °C (2104 cm^{-1}) could be due rather to formation of a metallic copper carbonyl.

In the case of Cu/MgAl-8, the spectra (Fig. 12) show the presence of isolated and associated hydroxyls (bands at ca. 3678 and 3400 cm^{-1}, respectively), carbonate species (two different species, according to the observed evolutions, giving bands at ca. 1539, 1404 and 1222 cm^{-1}, and ca. 1600 and 1374 cm^{-1}, respectively) and a relatively weak copper carbonyl at ca. 2102 cm^{-1} (note this appears

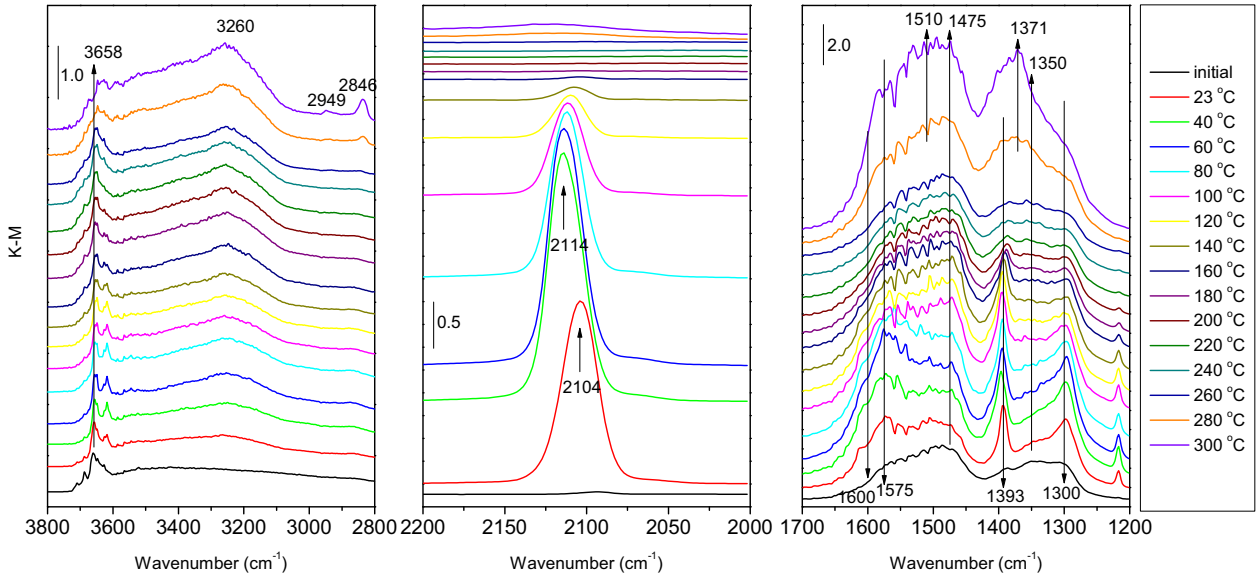

Fig. 11. DRIFTS spectra obtained under CO-PROX conditions (1% CO, 1.25% O_2 and 50% H_2 in He) over Cu/Ce-8 at the indicated temperatures. The spectrum at the bottom corresponds to that collected just before introduction of the reactant mixture.

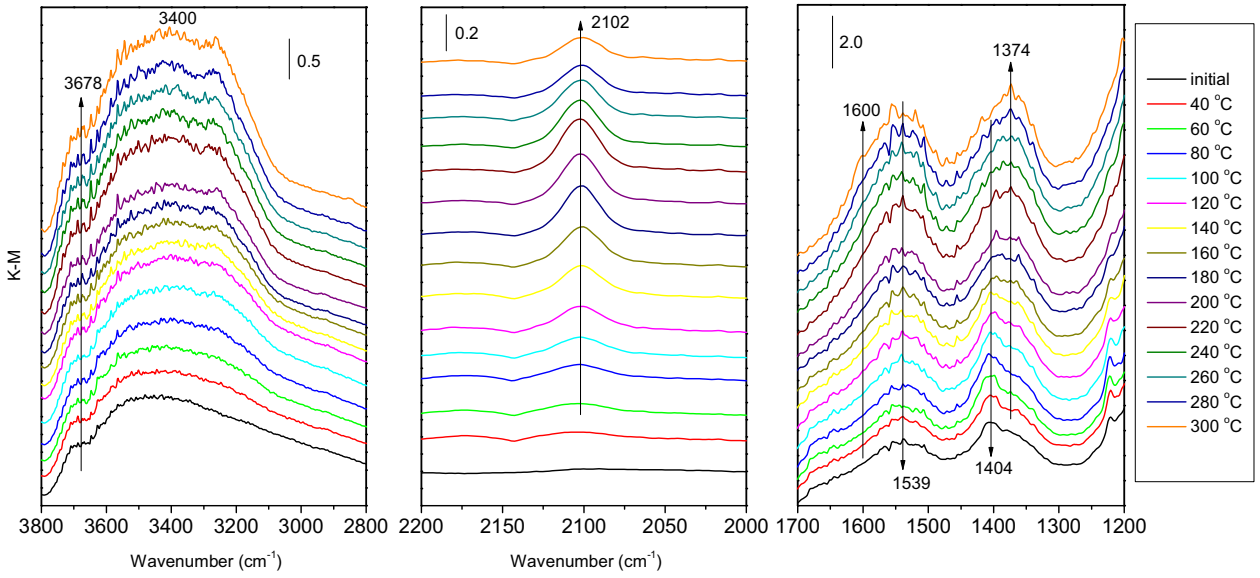

Fig. 12. DRIFTS spectra obtained under CO-PROX conditions (1% CO, 1.25% O_2 and 50% H_2 in He) over Cu/MgAl-8 at the indicated temperatures. The spectrum at the bottom corresponds to that collected just before introduction of the reactant mixture.

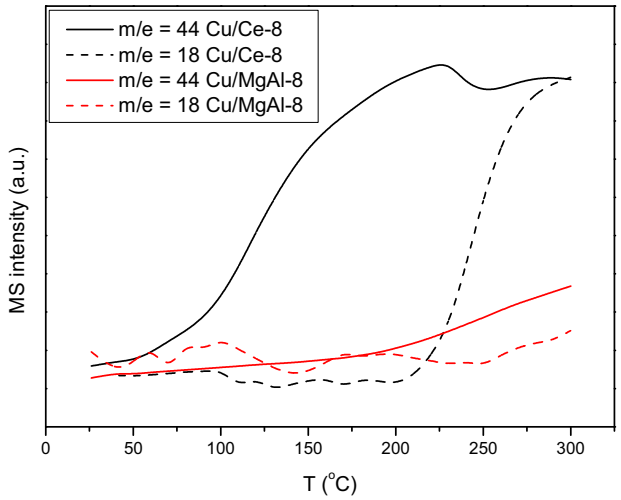

Fig. 13. Evolution of MS signals corresponding to CO_2 (m/e = 44) and H_2O (m/e = 18) during the course of CO-PROX DRIFTS experiments over Cu/Ce-8 and Cu/MgAl-8 (corresponding to spectra presented in Figs. 11 and 12).

overlapped on the two CO(g) bands centered at ca. 2143 cm^{-1}). This latter could be a metallic copper carbonyl according to its frequency [68]. It cannot however be discarded that it corresponds to a Cu^+ carbonyl given its relatively high thermal stability (even though at a relatively high p_{CO}, it still appears at 300 °C, which appears a temperature at which the lifetime of such carbonyl chemisorbed on metallic copper would be expected to be very short [69]). If this were the case, interaction with the basic support needs to be invoked in order to explain its relatively low frequency, taking into account such interaction would in principle favour a stronger π-back-bond component in the carbonyl, according to usual σ bond-π-back-bond scheme employed to explain carbonyl bonds in this type of species [70,71].

CO and H_2 oxidation activities observed during the DRIFTS experiments over the two reference samples reflect (in agreement with catalytic activity data obtained with the tubular reactor, Fig. 10; note that, despite qualitative coincidence is certainly reached, some differences appear when comparing activity data obtained with a more ideal tubular reactor, Fig. 10, and the DRIFTS cell reactor, Fig. 13, as a consequence of differences in the characteristics of each type of reactor) the significantly higher activity over Cu/Ce-8 for both reactions. The promoting effect of ceria on CO oxidation activity of CuO/CeO_2 catalysts has been generally related to its capability to promote the redox activity of CuO_x –CeO_{2-y} interfacial sites formed during the course of the interaction of the catalyst with the CO-PROX reactant mixture [29–31,52,62,72,73]. Cu^+ carbonyls as those shown in Fig. 11 have been proposed to constitute a signature of formation of such active sites given their intensity appears proportional to the CO oxidation rate [30,74]; note this rule is accomplished only when the interface is formed with ceria surfaces of similar morphological and chemical characteristics, properties which apparently determine importantly their redox and catalytic properties [31,38,52,54,75]. H_2 oxidation activity in copper/ceria catalysts under CO-PROX conditions has been correlated with achievement of a relatively high reduction level in the dispersed copper oxide particles during the course of the interaction of the catalyst with the reactant mixture [30]. This agrees with observation of onset of H_2 oxidation at a temperature just above which the Cu^+ carbonyls become extinguished under CO-PROX conditions [52]. This is also fairly accomplished in this case since such carbonyls apparently extinguish above 180 °C while onset of H_2 oxidation occurs around 200 °C (Figs. 11 and 13). Note such Cu^+ carbonyls would be expected to decrease with increasing temperature as a consequence of their thermal stability although they would still be expected to present appreciable intensity at around 200 °C, even considering that the p_{CO} would have decreased to around 1/10 of its initial value as a consequence of its transformation to CO_2, Fig. 13, if surface Cu^+ centers are exposed [64]. Then, considering that the catalyst must evolve towards more reduced states with increasing the temperature under the CO-PROX mixture [30], the extinction of the Cu^+ carbonyls taking place in Cu/Ce-8 above 180 °C can be interpreted as due to the formation of metallic states of copper, at least at surface level, whose carbonyls would eventually present relatively low thermal stability as to be observable at those relatively high temperatures [69]. The relatively low oxidation activity of Cu/MgAl-8 (Figs. 10 and 13) can be related first to the low activity of oxidized states of copper (in the absence of promoters like ceria) [47,76,77], most likely present in the initial oxidized catalyst. In second place, a relatively weak reduction level, which could give rise to more active states of copper [76], is

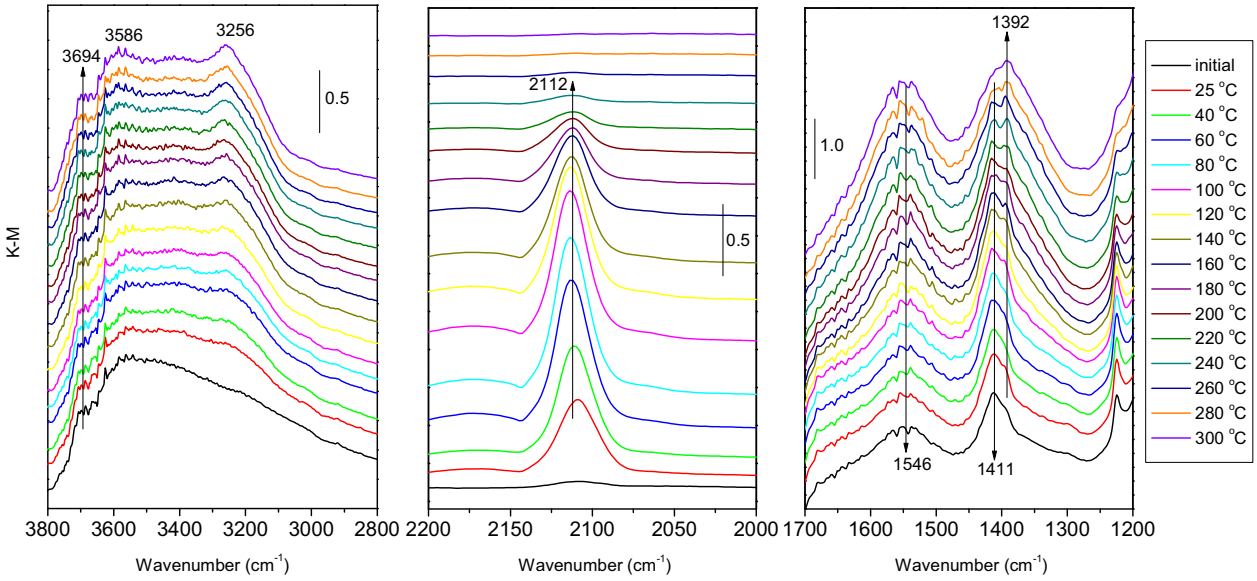

Fig. 14. DRIFTS spectra obtained under CO-PROX conditions (1% CO, 1.25% O_2 and 50% H_2 in He) over Cu/Ce/MgAl-8 at the indicated temperatures. The spectrum at the bottom corresponds to that collected just before introduction of the reactant mixture.

apparently achieved by copper under the reactant mixture in accordance with the weak intensity observed for the related carbonyl formed (Fig. 12). For both catalysts, carbonates are formed during the course of the process (Figs. 11 and 12). In the case of Cu/MgAl-8, they most likely arise from the interaction of CO_2, formed from CO oxidation, with the $MgAl_2O_4$ surface. For Cu/Ce-8, they could arise from interaction of either CO or CO_2 with the ceria surface (in principle, the carbonate-type species observed appear similar to those detected in the absence of copper) [64,66,67]. Apparently higher amount of these carbonate-type species are formed over Cu/Ce-8 in comparison with Cu/MgAl-8 most likely as a consequence of the higher reactivity of ceria and/or the higher CO oxidation activity of the former. In turn, a certain reorganization of hydroxyls is produced as a consequence of the interaction of the reactant mixture with Cu/Ce-8 at 23 °C. In particular, most basic hydroxyls apparently decrease most likely as a consequence of interaction with CO_2 and formation of the hydrogen carbonate species (note the decrease of hydroxyl bands around 3700 cm^{-1} concomitant to the increase of the hydrogen carbonate band at 3620 cm^{-1} along with associated ones in the CO stretching region). Some general increase in the intensity of bands due to hydroxyl species is also detected in any case already upon first interaction with the reactant mixture and which is attributed to the presence of ppm amount of water as impurity in the reactant gases. In the case of Cu/MgAl-8 only some increase in the intensity of hydroxyl species is observed at relatively high reaction temperature which could be due to the interaction with the water resulting from H_2 oxidation.

Fig. 14 shows the DRIFTS results for Cu/Ce/MgAl-8 at different reaction temperatures under the CO-PROX mixture. Concerning bands detected in the regions of hydroxyl and (more intense modes of) carbonate-type species, the spectra display important similarities with those observed for Cu/MgAl-8 (Fig. 12), thus suggesting it is mainly the $MgAl_2O_4$ component onto which such species are basically stabilized also in Cu/Ce/MgAl-8. This appears quite interesting since carbonates and hydroxyls are proposed to be involved as poisons of copper-ceria catalysts [78]; in this sense, experiments have been conducted in our laboratory in order to explore the possibilities of the $CuO/CeO_2/MgAl_2O_4$ catalysts under a CO-PROX mixture containing CO_2; details of such study fall out of the scope of the present work and will be presented in a separate contribution. In contrast to observations in the regions corresponding to hydroxyl- or carbonate-type species, which point towards formation of species mainly stabilized on the $MgAl_2O_4$ component of the support, the carbonyl region of the spectrum displays the formation of a Cu^+ carbonyl similar to those observed over Cu/Ce-8 (Fig. 11). The spectra observed under the same conditions for Cu/Ce/MgAl-4 and Cu/Ce/MgAl-10 displayed important similarities with those observed for Cu/Ce/MgAl-8 and are exhibited in a supplementary material file. Main difference found between them affects to respective intensity of the Cu^+-carbonyl related to species interacting with the CeO_2 component of the catalyst which, as discussed above, is of relevancy to explain respective CO oxidation activity, as will be discussed below. In this respect, Fig. 15 presents the evolution of gases representative of the two main oxidation reactions taking place during the CO-PROX process along with the evolution observed for the intensity of mentioned Cu^+-carbonyl species over the three $CuO/CeO_2/MgAl_2O_4$ catalysts.

3.3. *Structure/activity relationships in the $CuO/CeO_2/MgAl_2O_4$ catalysts*

Activity results obtained for the reference samples clearly evidence that most active sites for the process are constituted by contacts between copper and ceria while those established with $MgAl_2O_4$ are little active (Figs. 10 and 13). It is therefore of relevancy to examine first with which of the two components of the $CeO_2/MgAl_2O_4$ support has copper established corresponding contacts in the $CuO/CeO_2/MgAl_2O_4$ catalysts. These are basically formed during the preparation of the catalysts. In this sense, as shown elsewhere [39,41], the degree of interaction of the complexes present in the impregnating solution with the solid support surface depends on the PZC of the solid surface, i.e., in our case, in principle, of each of the two support components. This fact, as mentioned in the Introduction, motivated the selection of pH values for the impregnating solutions. The adsorption of the complexes in solution on the surface of the catalyst would thus be principally determined by respective charging degree achieved at the surface of the support components as well as the charge of the complexes in solution. Thus, for basic pH values, if dissolved anionic complexes were involved, the lower the PZC of the support component, the lower the complex uptake at its surface is expected. Opposite, for acid pH values, if cationic complexes were involved, the

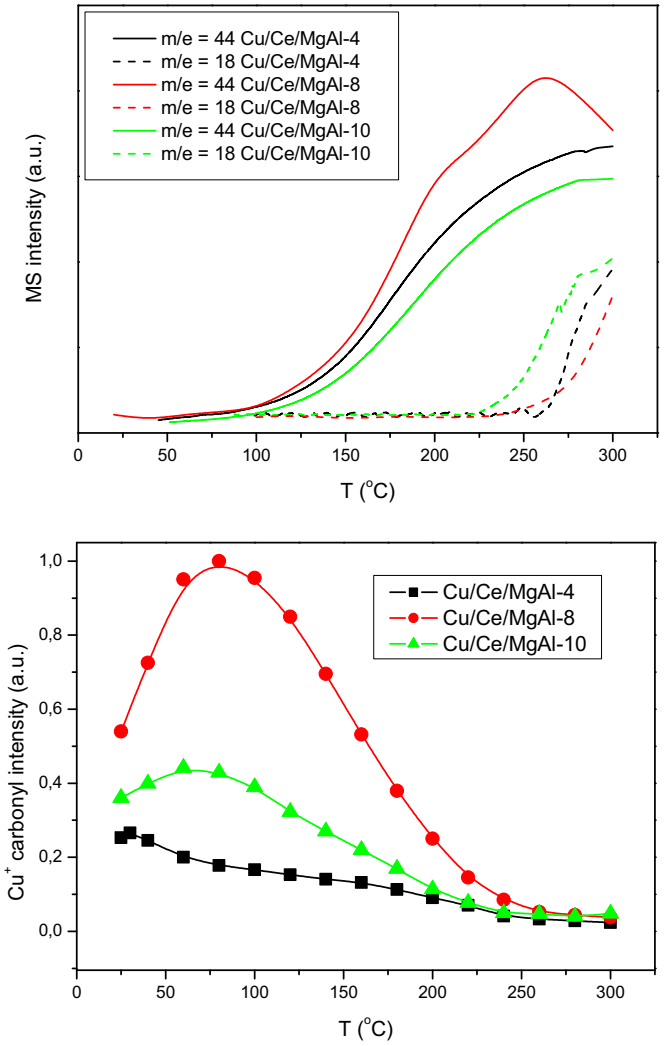

Fig. 15. Top: Evolution of MS signals corresponding to CO_2 (m/e = 44) and H_2O (m/e = 18) during the course of CO-PROX DRIFTS experiments over the indicated $CuO/CeO_2/MgAl_2O_4$ samples (corresponding to spectra presented in Fig. 14, S1 and S2). Bottom: Evolution of the intensity of species attributed to Cu^+-carbonyls during the course of corresponding DRIFTS tests under CO-PROX conditions.

lower the PZC of the support component, a higher complex uptake at its surface would be expected. It is therefore of relevancy the knowledge of the type of complexes present in the impregnating solutions employed. The pale blue color (Fig. 1) of the impregnating solution obtained at natural pH (pH = 4.0, according to the concentration employed to achieve incipient wetness conditions) upon dissolution of the copper nitrate precursor in water (as it occurs also when employing chloride precursor) is due to octahedral aquo-complexes of Cu^{2+} of the type $[Cu(H_2O)_6]^{2+}$; in turn, the deep blue colour achieved at pH = 10.0 upon addition of aqueous ammonia, Fig. 1, is attributable to the formation of $[Cu(NH_3)_4(H_2O)_6]^{2+}$ complexes [79]. At intermediate pH, in our case pH = 8, the presence of precipitated copper hydroxide is expected upon addition of ammonia. This explains the milky aspect of the blue dispersion obtained (Fig. 1). Then, considering PZC values of the two support components (see the Introduction), at pH = 4.0 it would be expected that the $[Cu(H_2O)_6]^{2+}$ complex adsorbs preferentially on the CeO_2 component. In turn, taking into account that a possitively charged copper complex ($[Cu(NH_3)_4(H_2O)_6]^{2+}$) is also expected to predominate in the solution prepared at pH = 10.0, it would be expected that it is also the CeO_2 component the one on which a preferential chemisorption of the complex is produced. XEDS mapping study of the catalysts confirms these trends since copper appears mainly associated to the ceria component of the catalyst for those two samples (Fig. 5). In contrast with those two situations, at pH = 8.0 a neutralization of the copper upon formation of the solid hydroxide is produced and the interaction of this with the support surface is most likely electrostatically weak. This justifies that no particular trend towards adsorption on any of the two support components is produced in that case and copper appears more homogeneously dispersed and more evenly distributed between the two support components in agreement with XEDS analysis (Fig. 5). XPS results also support these hypotheses when comparing Cu/Ce/MgAl-8 and Cu/Ce/MgAl-10 samples (Fig. 8 and Table 1). On the one hand, as discussed above, a reasonable interpretation of Cu 2p XPS features point in the same sense of a higher relative amount of copper species in contact with the ceria component for Cu/Ce/MgAl-10. Besides this, the lower [Cu]/([Cu] + [Ce] + [Al]) atomic ratio estimated from the XPS results for Cu/Ce/MgAl-10 (Table 1) could be also related to the higher trend of copper to form contacts with ceria in this sample which would result in an overall decrease in its dispersion degree with respect to Cu/Ce/MgAl-8 in which copper is more homogeneously distributed between the two support components.

However, despite the fact that a higher portion of the copper appears in contact with ceria in Cu/Ce/MgAl-10, this catalyst apparently presents lower CO oxidation activity than Cu/Ce/MgAl-8 while this appears also more active than Cu/Ce/MgAl-4 (Figs. 10 and 15) in which copper also appears to concentrate to a higher extent on the ceria component of the support (Fig. 5). Clearly there are other factors, further than the amount of contacts established between copper and ceria in each case, which are also most relevant to explain the catalytic properties of these systems. It must be noted also that, taking into account that the CO oxidation activity could be maximized at a certain loading of copper with respect to ceria, for wt% Cu/Ce ratio as for our catalysts, the CO oxidation rate is still expected to increase with the Cu/Ce ratio, before reaching a copper saturation amount above which the rate becomes practically constant [80,81]. The different catalytic activity results thus suggest different characteristics for the copper-ceria nanostructures established in each catalyst. Another evidence for this is provided by the H_2-TPR results (Fig. 7). Copper species interacting with ceria apparently reduce at higher temperature in Cu/Ce/MgAl-10. This does not appear to be, at least exclusively, related to possible lower dispersion degree of copper in it taking into account above discussed trend of copper to concentrate on ceria for this catalyst since Cu/Ce/MgAl-4 also presents such inhomogeneous distribution trend, as supported by XEDS mapping results (Fig. 5), while copper apparently reduces at lower temperature in this catalyst (Fig. 7).

The activity results reveal that optimum copper-ceria nanostructures are established when employing the impregnating dispersion at pH = 8.0. Indeed, the Cu/Ce-8 reference catalyst displays also remarkable catalytic activity when compared with analogous catalysts prepared under different conditions [24,29,52,62]. The highest CO oxidation activity of Cu/Ce/MgAl-8 correlates well with the stronger intensity observed for the Cu^+-carbonyl intensity (Fig. 15). As mentioned above, such intensity constitutes a fingerprint of the CO oxidation rate accomplished in each case in accordance with previous investigation [30]. However, this rule is apparently not fully accomplished in this case since Cu/Ce/MgAl-10 displays lower CO oxidation activity while it exhibits higher Cu^+-carbonyl intensity than Cu/Ce/MgAl-4 (Fig. 15). As discussed above, another condition for that rule is that the active CuO_x —CeO_{2-y} interfaces present comparable morphological and chemical properties [31,38,52]. A difference in this sense which can be also relevant to explain the activity differences is the size of the CeO_2 nanoparticles dispersed over the $MgAl_2O_4$

support. According to the analysis of the STEM-HAADF micrographs for the three samples, the average ceria size apparently decreases between Cu/Ce/MgAl-4 (3.4 nm) and the other two samples (around 2.5 nm), Fig. 4. This difference must be due to the fact that partial dissolution of ceria upon interaction with the impregnating solutions can be produced in some case when interacting at pH far from corresponding PZC [41]. Those sizes for ceria are close to the limit below which quantum effects may begin to affect appreciably the electronic properties of the nanocrystals [82]. One of the effects observed in the case of very small ceria nanocrystals is that reduced states of cerium (Ce^{3+}) might become stabilized at their surface [81]. This affects the electronic properties of ceria and could help to stabilize Cu^+ states as a consequence of a facilitated electron transfer between dispersed CuO_x and ceria [38]. Such effect could be enhanced upon decreasing the size of the ceria nanoparticles and could explain the mentioned discrepancy between CO oxidation rate and Cu^+-carbonyl intensity (Fig. 15), i.e. in principle, such correlation could still be valid when comparing Cu/Ce/MgAl-8 and Cu/Ce/MgAl-10 with similar size for the dispersed ceria nanoparticles but Cu/Ce/MgAl-4 probably presents relatively lower Cu^+-carbonyl intensity because of a less favoured $CuO_x \rightarrow$ ceria electron transfer in it. The same type of effect has been invoked for explaining the discrepancy observed when dealing with different exposed ceria faces in the nanoparticles [52,75]. Alternatively, taking into account that XPS results point towards the presence of a part of the copper as Cu^+ in the calcined Cu/Ce/MgAl-10 catalyst, it may occur that such Cu^+ sites present lower activity than reduced copper sites formed at the interface upon interaction with the CO-PROX mixture while they contribute to formation of Cu^+-carbonyls of a similar nature (in principle, no significant frequency difference appears for that carbonyl species when comparing Cu/Ce/MgAl-8 and Cu/Ce/MgAl-10 *operando*-DRIFTS spectra). In any case, the stabilization of such Cu^+ species in Cu/Ce/MgAl-10 cannot be related to differences in redox properties as a consequence of a different size in the dispersed ceria entities since Cu/Ce/MgAl-8 practically presents the same size. A possibility could be that they become stabilized as a consequence of mutual interaction with Ce^{3+} species lixiviated, as a consequence of interaction with the basic medium, from the support surface. Their readsorption on the catalysts surface would then lead to stabilized Cu^+–Ce^{3+} pairs (thus explaining the relatively higher amount of Ce^{3+} detected by XPS for Cu/Ce/MgAl-10) with lower redox and catalytic activity than sites formed at the copper-ceria interface during interaction with the CO-PROX mixture. The formation of such Cu^+–Ce^{3+} pairs would be in any case favored by the basic medium and the presence of ammonium complexes at pH = 10.0 and would be hindered at pH = 8.0 due to the neutralization of the copper complexes in the form of copper hydroxide, as discussed above.

Another effect of the difference in the size of the dispersed ceria nanoparticles and the redox interaction between CuO_x and ceria can be related to the CO_2 selectivity observed during the process. In principle, such electron transfer can help to retard the reduction of CuO_x under the CO-PROX stream [31,38]. Indeed, a difference between Cu/Ce/MgAl catalysts and the reference Cu/Ce-8 one is related to respective stability of the Cu^+-carbonyl under CO-PROX conditions. While in the latter, they practically disappear above 180 °C, they are still apparently present above such temperature in the Cu/Ce/MgAl catalysts. This suggests a higher difficulty for full copper reduction to metallic copper in the Cu/Ce/MgAl systems which might be related to such electronic effect. The hindering of CuOx reduction has been proposed to be beneficial to the selectivity because most active state for H_2 oxidation has been related to achievement of a relatively high reduced state in the copper component [30,38]. This is apparently accomplished when comparing Cu/Ce/MgAl-8 and Cu/Ce/MgAl-4, taking into account the larger size of dispersed ceria entities for the latter (Fig. 4). However, apparently extra factors must be invoked to explain the difference between Cu/Ce/MgAl-8 and Cu/Ce/MgAl-10 in this respect. For any reason, the type of copper-ceria contacts established in the latter case are also less selective than for any of the two other catalysts. The concentration of copper on the ceria component of the catalyst in such case could favor achievement of a relatively higher reduction degree in it under interaction with the CO-PROX mixture, despite the fact that H_2-TPR results point towards more difficult reduction of copper in it (Fig. 7). Note in this sense that differences in the redox properties of copper oxide may arise when comparing CO and H_2 as reductants and this could explain such fact [52]; certainly, further experiments focused to specific characterization of the CuO_x-ceria interfaces formed in each case are required to get more hints about such apparent discrepancies.

4. Conclusions

Three catalysts with the same amount of copper (1 wt.%) dispersed by impregnation on a $CeO_2/MgAl_2O_4$ support but differing in the pH employed for the impregnating solution (pH = 4.0, 8.0 and 10.0; achieved by changing the amount of aqueous ammonia added) have been prepared. The structural and chemical characteristics of the various components in the catalysts have been analyzed in detail on the basis of a multitechnique (XRD, S_{BET} measurement, HREM and associated techniques, XPS, H_2-TPR and EPR) study. The catalysts are shown to be basically constituted by oxidized copper entities whose distribution over the support depends on the pH of the impregnating solution employed. This is explained on the basis of the type of complexes or precipitates which could be present on respective impregnating solutions as well as differences in PZC values of the two support components. Thus, on the basis of HREM-XEDS mapping analysis of the samples and as supported also by XPS, it is shown that copper tends to concentrate on the ceria component for pH = 4.0 and 10.0 while it appears more homogeneously distributed over the two components of the support for the sample prepared at pH = 8.0. Despite such relatively lower amount of contacts established between copper and ceria in this catalyst and taking into account that, on the basis of independent experiments performed on reference samples using CeO_2 and $MgAl_2O_4$ separately as supports, such contacts are much more active than those established between copper and $MgAl_2O_4$, the catalyst prepared at pH = 8.0 is shown to present most optimum CO-PROX performance both in terms of CO oxidation activity as well as CO_2 selectivity during the process. The higher intensity of Cu^+-carbonyls related to species interacting with ceria in this catalyst, as revealed by DRIFTS experiments performed under CO-PROX conditions, correlate well with achievement of higher CO oxidation activity over it. In turn, differences in respective size of the dispersed ceria nanoparticles and how this could affect to redox interactions between dispersed CuO_x and ceria in each case as well as respective dispersion degree achieved for the dispersed CuO_x entities are invoked to explain the CO_2 selectivity differences observed.

Acknowledgements

Thanks are due to Ms. C.L. Bolívar-Díaz for the help provided during some of the catalytic activity measurements. Thanks are also due to ICP-CSIC Unidad de Apoyo for the measurement of a part of the characterization results presented. This work was funded by the Ministerio de Economía y Competitividad (Plan Nacional Project CTQ2012-32928). Support from EU COST CM1104 action is also acknowledged.

Appendix A. Supplementary data

Supplementary data associated with this article can be found, in the online version, at http://dx.doi.org/10.1016/j.apcatb.2016.02.011.

References

[1] J.R. Rostrup-Nielsen, J. Sehested, J.K. Norskov, Adv. Catal. 47 (2002) 65–138.
[2] R.A. Lemons, J. Power Source 29 (1990) 251–264.
[3] Q. Li, R. He, J.A. Gao, J.O. Jensen, N. Bjerrum, Electrochem. Soc. J. 150 (2003) A1599–A1605.
[4] C. Ratnasamy, J.P. Wagner, Catal. Rev. Sci. Eng. 51 (2009) 325–440.
[5] J.M. Zalc, D.G. Loffler, J. Power Source 111 (2002) 58–64.
[6] E.D. Park, D. Lee, H.C. Lee, Recent progress in selective CO removal in a H2-rich stream, Catal. Today 139 (2009) 280–290.
[7] N. Bion, F. Epron, M. Moreno, F. Mariño, D. Duprez, Top. Catal. 51 (2008) 76–88.
[8] S.H. Oh, R.M. Sinkevitch, J. Catal. 142 (1993) 254–262.
[9] C.D. Dudfield, R. Chen, P.L. Adcock, Int. J. Hydrogen Energy 26 (2001) 763–775.
[10] M.M. Schubert, M.J. Kahlich, H.A. Gasteiger, R.J. Behm, J. Power Source 84 (1999) 175–182.
[11] M.J. Kahlich, H.A. Gasteiger, R.J. Behm, J. Catal. 171 (1997) 93–105.
[12] M. Watanabe, H. Igarashi, M. Suzuki, Y. Sasaki, H. Uchida, Appl. Catal. A 159 (1997) 159–169.
[13] P.V. Snytnikov, V.A. Sobyanin, V.D. Belyaev, P.G. Tsyrulnikov, N.B. Shitova, D.A. Shlyapin, Appl. Catal. A 239 (2003) 149–156.
[14] I.H. Son, A.M. Lane, Catal. Lett. 76 (2001) 151–154.
[15] O. Korotkikh, R. Farrauto, Catal. Today 62 (2000) 249–254.
[16] S.H. Lee, J. Han, K.Y. Lee, J. Power Source 109 (2002) 394–402.
[17] I.H. Son, M. Shamsuzzoha, A.M. Lane, J. Catal. 210 (2002) 460–465.
[18] K. Cho, M.A. Vannice, Stud. Surf. Sci. Catal. 130 (2000) 2345–2356.
[19] G.K. Bethke, H.H. Kung, Appl. Catal. A 194–195 (2000) 43–53.
[20] M.M. Schubert, V. Plzak, J. Garche, R.J. Behm, Catal. Lett. 76 (2001) 143–150.
[21] R.J.H. Grisel, B.E. Nieuwenhuys, J. Catal. 199 (2001) 48–59.
[22] G. Avgouropoulos, T. Ioannides, H.K. Matralis, J. Batista, S. Hocevar, Catal. Lett. 73 (2001) 33–39.
[23] Y. Teng, H. Sakurai, A. Ueda, T. Kobayashi, Int. J. Hydrogen Energy 24 (1999) 355–358.
[24] A. Martinez-Arias, A.B. Hungria, M. Fernandez-Garcia, J.C. Conesa, G. Munuera, J. Power Source 151 (2005) 32–42.
[25] I. López, T. Valdés-Solís, G. Marbán, Int. J. Hydrogen Energy 33 (2008) 197–205.
[26] T. Avgouropoulos, Ch. Ioannides, J. Papadopoulou, S. Batista, H.K. Hocevar, Catal. Today 75 (2002) 157–167.
[27] W. Liu, A.F. Sarofim, M. Flytzani-Stephanopoulos, Chem. Eng. Sci. 49 (1995) 4871–4888.
[28] A. Martínez-Arias, M. Fernández-García, O. Gálvez, J.M. Coronado, J.A. Anderson, J.C. Conesa, J. Soria, G. Munuera, J. Catal. 195 (2000) 207–215.
[29] D. Gamarra, G. Munuera, A.B. Hungría, M. Fernández-Garcia, J.C. Conesa, P.A. Midgley, X.Q. Wang, J.C. Hanson, J.A. Rodriguez, A. Martínez-Arias, J. Phys. Chem. C 111 (2007) 11026–11038.
[30] D. Gamarra, C. Belver, M. Fernández-García, A. Martínez-Arias, J. Am. Chem. Soc. 129 (2007) 12064–12065.
[31] A. Kubacka, A. Martínez-Arias, M. Fernández-García, ChemCatChem 7 (2015) 3614–3624.
[32] B.M. Reddy, P. Saikia, P. Bharali, Catal. Surv. Asia 12 (2008) 214–228.
[33] J. Salmones, J.A. Galicia, J.A. Wang, M.A. Valenzuela, G. Aguilar-Rios, J. Mater. Sci. Lett. 19 (2000) 1033–1037.
[34] E. Moretti, M. Lenarda, L. Storaro, A. Talon, T. Montanari, G. Busca, E. Rodríguez-Castellón, A. Jiménez-López, M. Turco, G. Bagnasco, R. Frattini, Appl. Catal. A 335 (2008) 46–55.
[35] A. Martínez-Arias, M. Fernández-García, L.N. Salamanca, R.X. Valenzuela, J.C. Conesa, J. Soria, J. Phys. Chem. B 104 (2000) 4038–4046.
[36] R. Di Monte, P. Fornasiero, J. Kaŝpar, M. Graziani, J.M. Gatica, S. Bernal, A. Gómez-Herrero, Chem. Commun. (2000) 2167–2168.
[37] L. Cheng, D. Mei, Q. Ge, J. Phys. Chem. C 113 (2009) 18296–18303.
[38] A. Loípez Caímara, V. Corteís Corberaín, L. Barrio, G. Zhou, R. Si, J.C. Hanson, M. Monte, J.C. Conesa, J.A. Rodriguez, A. Martínez-Arias, J. Phys. Chem. C 118 (2014) 9030–9041.
[39] G.A. Parks, Chem. Rev. 65 (1965) 177–198.
[40] M. Kosmulski, J. Colloid Interface Sci. 337 (2009) 439–448.
[41] K.P. de Jong (Ed.), Synthesis of Solid Catalysts, Wiley-VCH, Weinheim, 2009.
[42] L.C. Chung, C.T. Yeh, Catal. Commun. 9 (2008) 670–674.
[43] Z. Liu, S. Yang, R. Zhou, X. Zheng, J. Nat. Gas Chem. 19 (2010) 313–317.
[44] M.D. Hernández-Alonso, A.B. Hungría, A. Martínez-Arias, J.M. Coronado, J.C. Conesa, J. Soria, M. Fernández-García, Phys. Chem. Chem. Phys. 6 (2004) 3524–3529.
[45] A. Martínez-Arias, M. Fernández-García, A.B. Hungría, J.C. Conesa, G. Munuera, J. Phys. Chem. B 107 (2003) 2667–2677.
[46] S.Y. Yao, W.Q. Xu, A.C. Johnston-Peck, F.Z. Zhao, Z.Y. Liu, S. Luo, S.D. Senanayake, A. Martínez-Arias, W.J. Liu, J.A. Rodriguez, Phys. Chem. Chem. Phys. 16 (2014) 17183–17195.
[47] A. Martínez-Arias, R. Cataluña, J.C. Conesa, J. Soria, J. Phys. Chem. B 102 (1998) 809–817.
[48] A. Martínez-Arias, M. Fernández-García, J. Soria, J.C. Conesa, J. Catal. 182 (1999) 367–377.
[49] A. Martínez-Arias, A.B. Hungría, M. Fernández-García, J.C. Conesa, G. Munuera, J. Phys. Chem. B 108 (2004) 17983–17991.
[50] F. Mehran, S.E. Barnes, G.V. Chandrashekhar, T.R. McGuire, M.W. Shafer, Sol. St. Commun. 67 (1988) 1187–1189.
[51] M.-F. Luo, J.-M. Ma, J.-Q. Lu, Y.-P. Song, Y.-J. Wang, J. Catal. 246 (2007) 52–59.
[52] D. Gamarra, A. López Cámara, M. Monte, S.B. Rasmussen, L.E. Chinchilla, A.B. Hungría, G. Munuera, N. Gyorffy, Z. Schay, V. Cortés Corberán, J.C. Conesa, A. Martínez-Arias, Appl. Catal. B 130–131 (2013) 224–238.
[53] S. Tsunekawa, T. Fukuda, A. Kasuya, Surf. Sci. 457 (2000) L437–L440.
[54] M. Monte, G. Munuera, D. Costa, J.C. Conesa, A. Martínez-Arias, Phys. Chem. Chem. Phys. 17 (2015) 29995–30004.
[55] J.P. Holgado, R. Alvarez, G. Munuera, Appl. Surf. Sci. 161 (2000) 301–315.
[56] C.D. Wagner, L.E. Davis, M.V. Zeller, J.A. Taylor, R.H. Raymond, L.H. Gale, Surf. Interf. Anal. 3 (1981) 211–225.
[57] C.D. Wagner, Faraday Discuss. Chem. Soc. 60 (1975) 291–300.
[58] G.J. Moretti, J. Elect, Spectrosc. Relat. Phenom. 95 (1998) 95–144.
[59] M. Fernández-García, E. Gómez Rebollo, A. Guerrero Ruiz, J.C. Conesa, J. Soria, J. Catal. 172 (1997) 146–159.
[60] J. Xiaoyuan, L. Liping, C. Yingxu, Z. Xiaoming, J. Mol. Catal. A 197 (2003) 193–205.
[61] L. Dong, Y. Hu, M. Shen, T. Jin, J. Wang, W. Ding, Y. Chen, Chem. Mater. 13 (2001) 4227–4232.
[62] A. Martínez-Arias, A.B. Hungría, M. Fernández-García, A. Iglesias-Juez, J. Soria, J.C. Conesa, J.A. Anderson, G. Munuera, Phys. Chem. Chem. Phys. 14 (2012) 2144–2151.
[63] G. Mattogno, G. Righini, G. Montesperelli, E. Traversa, J. Mater. Res. 9 (1994) 1426–1433.
[64] P. Bera, A. López Cámara, A. Hornés, A. Martínez-Arias, J. Phys. Chem. C 113 (2009) 10689–10695.
[65] G.N. Vayssilov, M. Mihaylov, P.S. Petkov, K.I. Hadjiivanov, K.M. Neyman, J. Phys. Chem. C 115 (2011) 23435–23454.
[66] C. Li, Y. Sakata, T. Arai, K. Domen, K. Maruya, T. Onishi, J. Chem. Soc. Faraday Trans. I 85 (1989) 929–943.
[67] C. Binet, M. Daturi, J.-C. Lavalley, Catal. Today 50 (1999) 207–225.
[68] P. Hollins, Surf. Sci. Rep. 16 (1992) 51–94.
[69] M.B. Padley, C.H. Rochester, G.J. Hutchings, F. King, J. Catal. 148 (1994) 438–452.
[70] E. Groppo, S. Bertarione, F. Rotunno, G. Agostini, D. Scarano, R. Pellegrini, G. Leofanti, A. Zecchina, C. Lamberti, J. Phys. Chem. C 111 (2007) 7021–7028.
[71] K.I. Hadjiivanov, M. Kantcheva, D.G. Klissurski, J. Chem. Soc. Faraday Trans. 92 (1996) 4595–4600.
[72] A. Martínez-Arias, D. Gamarra, M. Fernández-García, A. Hornés, P. Bera, Zs. Koppány, Catal. Today 143 (2009) 211–217.
[73] S. Yao, K. Mudiyanselage, W. Xu, A.C. Johnston-Peck, J.C. Hanson, T. Wu, D. Stacchiola, J.A. Rodriguez, H. Zhao, K.A. Beyer, K.W. Chapman, P.J. Chupas, A. Martínez-Arias, R. Si, T.B. Bolin, W. Liu, S.D. Senanayake, ACS Catal. 4 (2014) 1650–1661.
[74] C.S. Polster, H. Nair, C.D. Baertsch, J. Catal. 266 (2009) 308–319.
[75] M. Monte, D. Gamarra, A. López Cámara, S.B. Rasmussen, N. Gyorffy, Z. Schay, A. Martínez-Arias, J.C. Conesa, Catal. Today 229 (2014) 104–113.
[76] A. Martínez-Arias, J. Soria, R. Cataluna, J.C. Conesa, V. Cortés Corberán, Stud. Surf. Sci. Catal. 116 (1998) 591–600.
[77] G.G. Jernigan, G.A. Somorjai, J. Catal. 147 (1994) 567–577.
[78] D. Gamarra, A. Martinez-Arias, J. Catal. 263 (2009) 189–195.
[79] V.F. Anufrienko, R.A. Shutilov, G.A. Zenkovets, V.Y. Gavrilov, N.T. Vasenin, A.A. Shubin, T.V. Larina, A.V. Zhuzhgov, Z.R. Ismagilov, V.N. Parmon, Russ. J. Inorg. Chem. 57 (2012) 1285–1290.
[80] M.-F. Luo, Y.-J. Zhong, X.-X. Yuan, X.-M. Zheng, Appl. Catal. A 162 (1997) 121–131.
[81] A.-P. Jia, S.-Y. Jiang, J.-Q. Lu, M.-F. Luo, J. Phys. Chem. C 114 (2010) 21605–21610.
[82] M. Fernández-García, A. Martínez-Arias, J.C. Hanson, J.A. Rodriguez, Chem. Rev. 104 (2004) 4063–4104.